Mechanical properties and microstructural evolution of nanocrystalline titanium at elevated temperatures

Hamed Shahmir, Pedro Henrique R. Pereira, Yi Huang, Terence G. Langdon

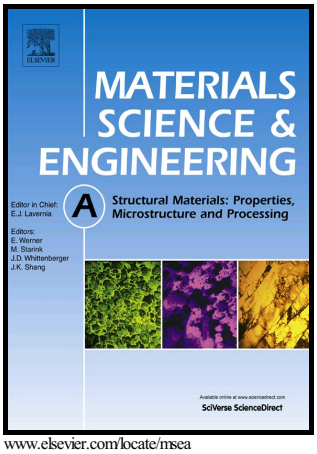

www.elsevier.com/locate/msea

PII: S0921-5093(16)30621-9
DOI: http://dx.doi.org/10.1016/j.msea.2016.05.105
Reference: MSA33733

To appear in: *Materials Science & Engineering A*

Received date: 20 April 2016
Revised date: 24 May 2016
Accepted date: 25 May 2016

Cite this article as: Hamed Shahmir, Pedro Henrique R. Pereira, Yi Huang and Terence G. Langdon, Mechanical properties and microstructural evolution of nanocrystalline titanium at elevated temperatures, *Materials Science & Engineering A,* http://dx.doi.org/10.1016/j.msea.2016.05.105

Submitted to Materials Science and Engineering A (April 2016): revised May 2016

Mechanical properties and microstructural evolution of nanocrystalline titanium at elevated temperatures

Hamed Shahmir[a], Pedro Henrique R. Pereira[a], Yi Huang[a], Terence G. Langdon[a,b]

[a] *Materials Research Group, Faculty of Engineering and the Environment, University of Southampton, Southampton SO17 1BJ, UK*
[b] *Departments of Aerospace & Mechanical Engineering and Materials Science, University of Southern California, Los Angeles, CA 90089-1453, USA*

Abstract

An investigation was initiated to study the mechanical properties and microstructural evolution of nanocrystalline titanium in the temperature range of 473-923 K after processing by high-pressure torsion (HPT) under a pressure of 5.0 GPa for up to 10 turns. The results show there is a significant improvement in both the tensile strength and the ductility in nanocrystalline Ti by comparison with coarse-grained (CG) Ti at elevated temperatures. The strength of HPT-processed Ti drops to that of CG Ti at temperatures above 773 K because of grain growth. An investigation of the mechanical behaviour at elevated temperatures reveals an increasing-decreasing-increasing trend in the elongations to failure with increasing temperature. An elongation of >130 % was achieved both at 673 K and above 773 K for the HPT-processed samples and this was significantly larger than for the CG Ti. The highest measured elongation was ~200% for the HPT-processed sample tested at 923 K. A good combination of strength and elongation to failure was achieved in the temperature range of 573-773 K after HPT processing.

Keywords: High temperature behavior; high-pressure torsion; nanostructured materials; severe plastic deformation; titanium

[*]Corresponding author. Tel.: +442380594438; E-mail address: H.Shahmir@soton.ac.uk

1. Introduction

Titanium (Ti) is an excellent metal for use in various areas of mechanical engineering and bioengineering due to its high corrosion resistance and biocompatibility [1,2]. Since pure Ti has low strength, alloying with other elements is generally used to increase its mechanical strength but this may lead to a degradation in the corrosion resistance and biocompatibility. This problem is especially acute for Ti because it is widely used for orthopedic and dental implants [3,4]. Nevertheless, it is now well established that achieving grain refinement through severe plastic deformation (SPD) may significantly improve the strength of metallic materials [5-7] and this includes pure Ti. In practice, these SPD processes are capable of hardening pure Ti whilst avoiding the additions of either solutes as in solid solution hardening or second phases as in precipitation hardening. It is reasonable to anticipate, therefore, that pure Ti processed by SPD will have high specific strength, high corrosion resistance and biocompatibility and therefore it will be an excellent candidate material for use in structural and bio-implant applications.

There are several different SPD techniques [8,9], but experiments show that processing by high-pressure torsion (HPT) is advantageous among these procedures because it produces materials having exceptionally small grain sizes [10,11] and larger fractions of grain boundaries having high angles of misorientation [12]. In this procedure, a disk-shaped specimen is deformed by simple shear between two anvils where it is constrained under a high pressure and subjected to concurrent torsional straining [6].

The post-deformation of nanostructured metals is important for producing desired shapes. Most nanostructured metals and alloys are reported to have high strengths but low ductilities [13] and therefore selecting appropriate high temperature operations may result in both good ductilities and high strengths. By contrast, very high temperatures or low strain rates may lead to increased recovery and thereby reduce the hardness. Although the formability can be

improved at elevated temperatures, a manufacturing process at warm temperatures is more economical and thus more desirable and also may reduce the oxidizing condition [14].

There are several reports on the effect of HPT processing on the microstructure and mechanical properties of commercial purity (CP) Ti [15-26] but there are very few reports on the high temperature mechanical properties of Ti after HPT. It was reported that during tensile tests at 673 and 873 K the flow stress was significantly reduced by comparison with HPT-processed samples due to easier dislocation movement and grain growth and elongations to failure of ~60% and >60% was reported at 673 and 873 K, respectively [27]. In addition, it was shown that tensile testing of HPT-processed Ti at 523 K produced very high strength but significantly reduced ductility after 1 turn but there was increased ductility (up to 38%) and slightly increased strength (up to 800 MPa) after 5 turns [28]. The mechanical testing of CP Ti at 673 K showed a maximum elongation to failure of ~130% at a strain rate of 1.0×10^{-4} s^{-1} for a specimen processed by HPT through 10 turns [29] and this is consistent with a recent review demonstrating the ability to achieve higher ductilities by conducting SPD processing to very high strains [30].

Based on the limited information at present available on the high temperature properties of HPT-processed Ti, the present research was initiated with the objective of evaluating the evolution of microstructure and the mechanical properties of CP Ti in the temperature range of 473-923 K after processing by HPT.

2. Experimental material and procedures

The experiments were conducted using CP grade 2 titanium (99.2 % purity) that was received in the form of rods having diameters of 10.0 mm. These rods were annealed for 2 h at 973 K under an Ar-controlled atmosphere, furnace cooled and then cut into disks with thicknesses of ~0.8 mm. All disks were processed by HPT at room temperature under an applied pressure, *P*, of 5.0 GPa, a rotation speed of 1 rpm and torsional straining through

numbers of revolutions, *N*, of 1, 5 and 10 turns. The HPT facility operated under quasi-constrained conditions in which there is a small outflow of material around the periphery of the disk during the processing operation [31,32].

Following HPT, each disk was polished to a mirror-like quality and hardness measurements were taken using a Vickers microhardness tester with a load of 500 gf and a dwell time of 10 s. The average microhardness values, Hv, were measured along randomly selected diameters on each disk. These measurements were taken at intervals of 0.5 mm, and at every point the local value of Hv was obtained from the average of four separate hardness values. X-ray diffraction (XRD) (Rigaku SmartLab) was used to study the phases after HPT employing Cu Kα radiation (wavelength $\lambda = 0.154$ nm) at 45 kV and a tube current of 200 mA. The XRD measurements were carried out over an angular 2θ range from 30° to 90° using a scanning step of 0.01° and a scanning speed of 2 deg min^{-1}. Differential scanning calorimetery (DSC) analysis was performed with a Mettler-Toledo instrument using non-isothermal (scanning) experiments upon heating at a scanning rate of 10 K min^{-1} in the temperature range of 298-773 K. Sample areas with diameters of 3 mm located near the edges of the disks were analyzed using DSC and XRD. A foil was prepared for scanning transmission electron microscopy (STEM) using a focused ion beam (FIB) facility (Zeiss Nvision 40) at 3 mm from the disk centre in the normal section of the disk so that the normal of the image was in the shear direction.

Two miniature tensile specimens were cut from symmetric off-centre positions in each disk near the edges using electro-discharge machining. This specimen configuration was described earlier with gauge dimensions of 1.1 × 1.0 × 0.6 mm^3 [33]. The mechanical properties were examined at room temperature after HPT processing through different numbers of turns and at elevated temperatures in the range from 473 to 923 K at 50 K intervals. In addition, and for comparison purposes, the mechanical properties of annealed coarse-grained (CG) Ti were examined in the temperature range of 473 to 873 K at 100 K intervals. All

specimens were heated rapidly to the testing temperature, typically in a time of ~5-10 min, and then held for 10 min to reach a uniform temperature prior to testing. Stress-strain curves were recorded using an initial strain rate of 1.0×10^{-3} s^{-1}. The stress-strain curves were plotted for each specimen and the yield stress (YS) and ultimate tensile strength (UTS) were then measured from each curve. At least two samples were tested for each condition. All elongations were carefully calculated by measuring the gauge lengths before and after tensile testing using an optical microscope.

The microstructures of samples after tensile testing at elevated temperatures were characterized by scanning electron microscopy (SEM) and electron backscattered diffraction (EBSD) analysis using a JSM6500F thermal field emission scanning electron microscope. The EBSD patterns were collecting using step sizes of 45, 180 and 450 nm for the samples pulled to failure at 673, 773 and 873 K, respectively. Low-angle grain boundaries (LAGBs) were defined as boundaries having misorientation differences between adjacent measuring points within the range from 2 to 15^{o} and high-angle grain boundaries (HAGBs) had misorientation differences of more than 15°. A clean-up procedure including grain dilatation and grain confidence index standardization was performed on each EBSD image such that the total numbers of modified points were less than 20 % for all measured points.

3. Experimental results

3.1 Microstructures and mechanical properties after HPT processing

The results for the corresponding Vickers microhardness measurements are shown in Fig. 1(a) for a rotation speed of 1 rpm after processing through different numbers of turns with the average values of Hv plotted along each disk diameter and with the lower dashed line at Hv ≈ 170 corresponding to the initial hardness in the annealed condition. Inspection of Fig. 1(a) shows that the hardness at the edges of the disks increases significantly after 1 turn such that, with reference to the annealed condition, there is an increase in the hardness value by a factor of ~1.7 up to Hv ≈ 280. By contrast, the hardness in the centre of the disks increases only from

the annealed value of Hv ≈ 170 to a value of Hv ≈ 230. The hardness values at the peripheries of the disks increase up to Hv ≈ 300 after 5 and 10 turns and in the centres the hardness values gradually increase up to Hv ≈ 280 with increasing N to 10 turns. These results confirm the development of a gradual evolution in hardness across the disk diameters with increasing torsional straining. Although, the hardness is lower at the centre than at the edges of the disk at N = 1, the hardness tends to become more homogeneous with increasing numbers of turns.

Figure 1(b) shows the X-ray diffraction patterns at the edges of the disks of the CP-Ti after HPT for different numbers of rotations. Earlier results in a fully-annealed condition without HPT processing showed that, as anticipated, the initial microstructure consisted only of the α-phase Ti. Nevertheless, ω-phase peaks, with the main peak position corresponding to the (101) at the 2θ = 39° coordinate, are clearly revealed after processing by HPT for 5 turns and this confirms the occurrence of an α to ω transformation. It is well known that the α to ω-phase transformation occurs under high pressure at ambient temperature but the resultant ω-phase is not stable [34]. Also, straining under a high pressure leads to the formation and stabilization of the ω-phase at ambient conditions [22-25]. The crystal structure of the ω-phase is based on a regular hexagonal closed-packed atomic lattice but with an open structure in which there are only 3 atoms per unit cell at the (0, 0, 0), (1/2, 2/3, c/2a), and (2/3, 1/3, c/2a) positions where c and a are the lattice parameters. This phase transformation significantly affects the mechanical properties of Ti and leads to an increase in the hardness and strength [22,23]. The present results in Fig. 1(b) show that the intensities of the ω-phase peaks increase with increasing torsional straining. The volume fractions of the ω-phase after HPT processing were calculated using standard procedures [35] and these calculations showed that the ω-phase volume fraction increased from 0 to ~27% when the numbers of rotations increased from 1 to 10 turns.

The microstructure of CP-Ti before and after 10 turns of HPT processing are recorded in Fig. 2 at distances of about 3 mm from the disk centres. The microstructure before HPT processing in Fig. 2(a) is typical of a fully-annealed sample consisting of equiaxed grains with

an average grain size of ~65 μm. After 10 turns of HPT processing in Fig. 2(b), the microstructure consists of small equiaxed grains with an average nanocrystalline size of ~70 nm and with many of the grains surrounded by curved or ill-defined grain boundaries. Much strain contrast is visible within these very small grains and this is associated with the presence of dislocations. Observations of diffuse boundaries between highly-deformed grains is typical of the microstructures generally visible after SPD processing due to the presence of many non-equilibrium boundaries containing extrinsic dislocations [36].

The stress-strain curves for the CP-Ti tested at room temperature are shown in Fig. 3 for an initial strain rate of 1.0×10^{-3} s^{-1} in the fully-annealed condition where $N = 0$ and after processing by HPT through 1, 5 and 10 turns. It is apparent that HPT processing of CP-Ti leads to a significant increase in strength but a sharp decrease in ductility. Furthermore, there is a minor increase in strength but a major decrease in ductility with additional straining. Thus, the highest strength of ~945 MPa and the lowest elongation of ~9% correspond to the sample processed through 10 turns.

3.2 Mechanical properties and microstructural evolution at elevated temperatures

The stress-strain curves at elevated temperatures (473-923 K) for HPT-processed samples after 10 turns and for annealed CG samples at an initial strain rate of 1.0×10^{-3} s^{-1} are shown in Fig. 4(a) and (b), respectively, with the curves at room temperature also included for comparison. Thus, the flow behavior of the nanocrystalline Ti at elevated temperatures in Fig. 4(a) shows significant strain hardening at temperatures below 673 K but at higher temperatures there is a reasonably steady-state behavior. The UTS and the elongation to failure are plotted as a function of the testing temperature in Fig. 5(a) and (b), respectively. Thus, the UTS decreases and at the highest testing temperatures the values of the UTS are essentially identical for both the CG and the nanocrystalline material. For the elongations to failure, both the annealed CG Ti and the nanocrystalline Ti show an increase with increasing temperature up to about 673 K and then a slight decrease to 773 K followed by a further increase. These results clearly show a very

significant improvement in the mechanical properties of CP-Ti at elevated temperatures after HPT processing with elongations of more than 100% at temperatures at and above about 573 K.

Non-isothermal DSC measurements are shown in Fig. 6(a) for the CP Ti at the edge of a disk processed through 10 turns and these results suggest the appearance of an exothermic peak on the DSC thermogram which disappears during heating in the second run. The appearance of the exothermic peak is related to the occurrence of recovery and recrystallization after HPT processing and the curve suggests that recovery and recrystallization start at temperatures of ~556 K and ~650 K, respectively. Fig. 6(b) shows results for Vickers microhardness measurements in the grip sections of the samples plotted after tensile testing at different temperatures following HPT processing through 10 turns. This plot confirms that the hardness of the nanocrystalline Ti decreases slightly after holding at high temperatures up to 623 K due to activation of a recovery mechanism and then it decreases significantly at higher temperatures due to the occurrence of recrystallization up to 773 K. Finally, the hardness reaches the level of the fully-annealed condition after 873 K due to grain growth. A general inspection of Fig. 6 shows that there is a good correlation between the DSC results in Fig. 6(a) and the microhardness measurements in Fig. 6(b).

The microstructures of nanocrystalline samples pulled to failure at 673, 773 and 873 K are shown in Fig. 7 where these micrographs were recorded within the gauge sections but very close to the fracture points. These images show that the microstructures of the samples deformed at 673 and 773 K consist of equiaxed fine grains whereas after tension at 873 K there are elongated coarse grains. Thus, the grain size increases with increasing test temperature and it is important to note also that some small cavities are visible in the microstructure of the sample deformed at 773 K whereas there appeared to be no cavitation in the samples tested at higher temperatures.

Figure 8 shows the EBSD-orientation images of tensile specimens after testing at 673, 773 and 873 K for the grip section shown in the left column and the gauge area shown in the right

column: information on the grain sizes, *d*, and the fractions of HAGB and LAGB are given along the lower edge of each image. A homogeneous equiaxed microstructure with random crystallographic orientations was present in the grip section after testing at 673-873 K and in the gauge section after testing at 673 and 773 K. A comparison of the undeformed and deformed microstructures in Fig. 8 (a) and (b) reveals the presence of slightly larger grains in the gauge section and therefore in the deformed region and most of these grains are reasonably equiaxed although the specimen was deformed to an elongation of ~130%. In Fig. 8 (c) and (d) the grains are equiaxed in both areas of the sample at 773 K with similar grain sizes close to ~ 1 μm and in Fig. 8 (e) and (f) there is very significant grain coarsening to ~9 μm in the gauge section at 873 K and the fraction of LAGBs tends to increase after tensile deformation at this temperature.

4. Discussion

In order to obtain large deformation, it is necessary to deform CP-Ti at higher temperatures where non-basal slip systems become activated to provide improved ductility [37]. This situation is more critical in nanostructured Ti where there is high strength and low ductility. The hexagonal close-packed α-phase is the stable phase during deformation of both CG and nanocrystalline Ti at elevated temperatures (473-923 K) because there is an ω to α reverse phase transformation at temperatures above ~423 K [22] and an α to β phase transformation with a body-centered cubic crystal structure at temperatures above ~1155 K [34].

In the following sections, the mechanical properties and microstructures are examined within different temperature ranges.

4.1 Mechanical behavior and microstructural evolution at temperatures below 673 K

Deformation twinning is the primary deformation mechanism at low temperatures but no twins are observed when the temperature reaches ~523 K [37]. As the temperature increases, the numbers of twins decrease dramatically so that slip becomes the dominant deformation mechanism accommodating the tensile strain. This explains the absence of twinning in this

study in the microstructures of specimens tested at temperatures at and above 673 K (Figs. 7 and 8).

It is apparent from Fig. 4(a) that nanocrystalline Ti shows significant strain hardening at the lower testing temperatures below ~673 K which suggests that dislocations accumulate in the recovered microstructure during deformation at these temperatures. The microstructural observations demonstrate that recrystallization starts at 673 K and this will lead to the nucleation and growth of fine dislocation-free grains [38]. The ultrafine-grained (UFG) microstructure visible after testing at 673 K and also the Vickers microhardness values plotted in Fig. 6 provide confirmation that this temperature is close to the onset of recrystallization. However, a comparison of Figs 8(a) and (b) shows that the grain size in the gauge area is significantly larger than in the grip area. In practice, the temperature for the onset of recrystallization decreases as the strain increases [38] and the stored energy during mechanical testing, which provides the driving force for recrystallization, increases with strain. Therefore, nucleation and growth are more rapid and occur at a lower temperature in the deformed material, thereby leading to the formation of larger grains in the deformed part of the sample after testing at 673 K.

The results in Fig. 5(b) show that the elongations to failure increase with temperature to an initial peak value at 673 K where this is due to the very small grain size produced by HPT processing and the recrystallization during heating. In addition, the occurrence of dynamic recovery may accommodate the strain during testing and lead to a high elongation at 673 K.

4.2 Mechanical behavior and microstructural evolution at temperatures from 673 to 773 K

In this temperature range the samples show a steady-state flow behavior and the elongations to failure decrease with a further increase in temperature to 773 K. During the initial stages of deformation, there is an increase in the flow stress as dislocations interact and multiply in the recrystallized microstructure. At a certain strain, the rates of strain hardening and recovery reach a dynamic equilibrium, the dislocation density remains constant and a

steady-state flow stress is obtained [38]. Such behavior is observed in Fig. 4 for the test at 773 K. The fundamental mechanisms of dynamic recovery are dislocation climb, cross-slip and glide and this leads to the formation of LAGBs as in static recovery [38]. This is reflected by the higher volume fraction of LAGBs in the gauge length (14%) by comparison with the undeformed grip section (8%).

Nevertheless, the formation of a grain size of <1μm may lead to changes in the deformation mechanism and the advent of some limited grain boundary sliding. Thus, grain refinement during static recrystallization before the tensile testing may facilitate the occurrence of sliding and thereby reduce the effective stress leading to flow softening.

The presence of equiaxed grains in both the undeformed and deformed parts of the sample at 773 K, as shown in Fig. 8(c) and (d), suggests that sliding may occur at this temperature but the relatively low elongation of ~100% suggest that sliding is not the rate-controlling mechanism under these conditions. During grain boundary sliding, the individual grains flow over each other in response to the applied stress but sliding cannot occur in isolation without opening up cavities in the material [39] and the growth and coalescence of voids under the applied stress will lead to significant decreases in the elongations to failure [40]. The occurrence of cavitation is clearly evident in the microstructure of the sample tested at 773 K as shown in Fig 7(b) and this is consistent with the decreased elongation to failure at this temperature.

It is important to recognize that a lower elongation was also attained in the CG material after testing at 773 K as shown in Fig. 5(b). This drop in elongation is associated with the classic “blue brittle” temperature [41.42] that is widely documented in Ti where minimum elongations occur at temperatures of ~750 K when testing at normal crosshead speeds. Thus, the results in Fig. 5(b) show that both CG and UFG Ti exhibit elongation drops at 773 K and then increases at temperatures above 773 K but the UFG Ti exhibits higher elongations to failure than the CG material. These results suggest that a UFG microstructure is probably

beneficial in diminishing the blue brittleness effect.

It is important to note also that there was no evidence for dynamic recrystallization at testing temperatures of 673-773 K. It is evident from Fig. 4(a) that the stress-strain curves in dynamic recrystallization generally exhibit a broad peak and this is different from the plateau which is characteristic of a material experiencing only dynamic recovery. Thus, it is reasonable to conclude there is no driving force for dynamic recrystallization during deformation at 673-773 K due to the occurrence of dynamic recovery and some limited grain boundary sliding.

4.3 Mechanical behavior and microstructural evolution at temperatures above 773 K

At higher temperatures, from 773 to 923 K, there is a strain hardening behaviour again. This corresponds to grain growth and the accumulation of dislocations as shown in Fig. 8 (f). The elongations to failure increase with temperature above 773 K as shown in Fig. 5(b) and these larger tensile elongations above the "blue brittle" temperature are a consequence of the grain growth. The results in Fig. 8(e) and (f) show remarkable grain growth in the gauge length at 873 K and a very significant increase in the fraction of LAGBs to 55%.

4.4 Pictorial representation of the microstructural changes

It is appropriate to summarize these findings by developing a pictorial representation denoting the true stress-true strain behaviour and the corresponding microstructures of samples tested at elevated temperatures. This is shown in Fig. 9 where the EBSD-orientation images are also shown at the same scale where each image has a diameter of 10 μm.

The mechanical properties at elevated temperatures show that both the tensile strength and the ductility increase up to 10 turns of HPT processing. The highest measured elongation in these experiments was ~200% for the sample processed by HPT through 10 turns and tested at 923 K using an initial strain rate of 1.0×10^{-3} s^{-1}. This elongation is outside of the superplastic regime which requires a minimum elongation of 400% [43] and therefore superplastic flow was not achieved in the CP-Ti after HPT. This observation is consistent with the results of

mechanical testing at 673 K which gave a maximum elongation to failure of ~130% at 1.0×10^{-4} s^{-1} for a specimen processed by HPT through 10 turns [29].

The strength values of the HPT-processed samples increased at a faster rate than the CG samples at temperatures below 823 K as shown in Fig. 5(a). In addition, elongations to failure of >130 % were achieved at 673 K and above 773 K after HPT processing and this is consistently higher than in the CG samples. Thus, it is concluded that the HPT-processed CP Ti exhibits a good combination of strength and ductility at temperatures in the range of 573-773 K. In addition, deformation in this temperature range as a warm deformation may be economical and thus more desirable and also may reduce the oxidizing condition.

5. Summary and conclusions

1. A CP Ti was processed by HPT under a pressure of 5.0 GPa up to 10 turns. Microstructural examination revealed an α to ω-phase transformation by increasing the numbers of rotations and there was significant grain refinement from an initial annealed value of ~65 μm to a grain size of ~70 nm. The results showed high hardness (300 Hv) and strength (940 MPa) in the nanocrystalline Ti.

2. The mechanical properties at 473-923 K gave a decreasing tensile strength with increasing temperature and the flow behaviour indicated hardening by dislocation accumulation in the recovered microstructures at temperatures below 673 K. At 673-773 K there was softening due to dynamic recovery and some limited grain boundary sliding. Grain growth and the accumulation of dislocations gave hardening at temperatures of 773-923 K.

3. The elongations to failure increased with temperature, reached a peak at 673 K and then decreased with an increase in temperature to 773 K and increased again at even higher temperatures. The decrease in elongation to failure at 773 K was attributed to cavity formation and blue brittleness.

4. The HPT-processed Ti samples exhibited a good combination of strength and ductility in the temperature range of 573-773 K. An elongation of >130 % was achieved at 673

K and at temperatures above 773 K after HPT processing and this was substantially higher than in the CG Ti.

Acknowledgements

The authors thank the Southampton Nanofabrication Center for preparing TEM samples using FIB. This work was supported by CAPES in Brazil (PHRP) and by the European Research Council under Grant Agreement No. 267464-SPDMETALS.

References

[1] R. Boyer, G. Welsch, E. Collings (eds.), *Materials Properties Handbook: Titanium Alloys*, ASM International, Materials Park, OH, 1998.

[2] C. Leyens, M. Peters, *Titanium and Titanium Alloys Fundamentals and Applications*, Wiley, Darmstadt, Germany, 2003.

[3] C.N. Elias, J.H.C. Lima, R. Valiev, M.A. Meyers, Biomedical applications of titanium and its alloys, JOM 60 (3) (2008) 46-49.

[4] M. Geetha, A.K. Singh, R. Asokamani, A.K. Gogia, Ti based biomaterials, the ultimate choice for orthopaedic implants - a review, Prog. Mater. Sci. 54 (2009) 397-425.

[5] R.Z. Valiev, T.G. Langdon, Principles of equal-channel angular pressing as a processing tool for grain refinement, Prog. Mater. Sci. 51 (2006) 881-981.

[6] A.P. Zhilyaev, T.G. Langdon, Using high-pressure torsion for metal processing: Fundamentals and applications, Prog. Mater. Sci. 53 (2008) 893-979.

[7] T.G. Langdon, Twenty-five years of ultrafine-grained materials: Achieving exceptional properties through grain refinement, Acta Mater. 61 (2013) 7035-7059.

[8] R.Z. Valiev, R.K. Islamgaliev, I.V. Alexandrov, Bulk Nanostructured Materials from Severe Plastic Deformation, Prog. Mater. Sci. 45 (2000) 103-189.

[9] R.Z. Valiev, Y. Estrin, Z. Horita, T.G. Langdon, M.J. Zehetbauer, Y.T. Zhu, Producing bulk ultrafine-grained materials by severe plastic deformation, JOM 58 (4) (2006) 33-39.

[10] A.P. Zhilyaev, B.K. Kim, G.V. Nurislamova, M.D. Baró, J.A. Szpunar, T.G. Langdon, Orientation imaging microscopy of ultrafine-grained nickel, Scr. Mater. 46 (2002) 575-580.

[11] A.P. Zhilyaev, G.V. Nurislamova, B.K. Kim, M.D. Baró, J.A. Szpunar, T.G.Langdon, Experimental parameters influencing grain refinement and microstructural evolution during high-pressure torsion, Acta Mater. 51 (2003) 753-765.

[12] J. Wongsa-Ngam, M. Kawasaki, T.G. Langdon, A comparison of microstructures and mechanical properties in a Cu-Zr alloy processed using different SPD techniques, J. Mater. Sci. 48 (2013) 4653-4660.

[13] C.C. Koch, Optimization of strength and ductility in nanocrystalline and ultrafine grained metals, Scr. Mater. 49 (2003) 657-662.

[14] L.C. Tsao, H.Y. Wu, J.C. Leong, C.J. Fang, Flow stress behavior of commercial pure titanium sheet during warm tensile deformation, Mater. Des. 34 (2012) 179-184.

[15] A.A. Popov, I.Yu. Pyshmintsev, S.L. Demakov, A.G. Illarionov, T.C. Lowe, A.V. Sergeyeva, R.Z. Valiev, Structural and mechanical properties of nanocrystalline titanium processed by severe plastic deformation, Scr. Mater. 37 (1997) 1089-1094.

[16] V.V. Stolyarov, Y.T. Zhu, T.C. Lowe, R.K. Islamgaliev, R.Z. Valiev, Processing nanocrystalline Ti and its nanocomposites from micrometer-sized Ti powder using high pressure torsion, Mater. Sci. Eng. A 282 (2000) 78-85.

[17] A.V. Sergueeva, V.V. Stolyarov, R.Z. Valiev, A.K. Mukherjee, Advanced Mechanical Properties of. Pure Titanium with Ultrafine Grained Structure, Scr. Mater. 45 (2001) 747-752.

[18] R.Z Valiev, A.V.Sergueeva, A.K. Mukherjee, The effect of annealing on tensile

deformation behavior of nanostructured SPD titanium, Scr. Mater. 49 (2003) 669-674.

[19] Y.Todaka, J. Sasaki, T. Moto, M. Umemoto, Bulk submicrocrystalline ω-Ti produced by high-pressure torsion straining, Scr. Mater. 59 (2008) 615-618.

[20] Y. Ivanisenko, A. Kilmametov, H. Rösner, R.Z. Valiev, Evidence of α→ω phase transition in titanium after high pressure torsion, Int. J. Mater. Res. 99 (2008) 36-41.

[21] R.K. Islamgaliev, V.U. Kazyhaniv, L.O. Shestakova, A.V. Sharafutdinov, R. Z. Valiev, Microstructure and mechanical properties of titanium Grade 4 processed by high pressure torsion, Mater. Sci. Eng. A 493 (2008) 190-194.

[22] Y. Todaka, M. Umemoto, A. Yamazaki, J. Sasaki, K. Tsuchiya, Effect of strain path in high-pressure torsion process on hardening in commercial purity titanium, Mater. Trans. 49 (2008) 47-53.

[23] K. Edalati, E. Matsubara, Z. Horita, Processing pure Ti by high-pressure torsion in wide ranges of pressures and strain, Metall. Mater. Trans. A 40 (2009) 2079-2086.

[24] A.V. Podolskiy, C. Mangler, E. Schafler, E.D. Tabachnikova, M.J. Zehetbauer, Microstructure and mechanical properties of high purity nanostructured titanium processed by high pressure torsion at temperatures 300 and 77 K, J. Mater. Sci. 48 (2013) 4689-4697.

[25] K. Edalati, T. Daio, M. Arita, S. Lee, Z. Horita, A.Togo, I. Tanaka, High-pressure torsion of titanium at cryogenic and room temperatures: Grain size effect on allotropic phase transformations, Acta Mater. 68 (2014) 207-213.

[26] C.T. Wang, A.G. Fox, T.G. Langdon, Microstructural evolution in ultrafine-grained titanium processed by high-pressure torsion under different pressures J. Mater. Sci. 49 (2014) 6558-6564.

[27] V.V. Stolyarov, Y.T. Zhu, T.C. Lowe, R.K. Islamgaliev, R.Z. Valiev, A two step SPD processing of ultrafine-grained titanium, Nanostruct. Mater. 11 (1999) 947-954.

[28] R.Z. Valiev, I.V. Alexandrov, Y.T. Zhu, T.C. Lowe, Paradox of strength and ductility in metals processed by severe plastic deformation, J. Mater. Res. 17 (2002) 5-8.

[29] M. Shirooyeh, J. Xu, T.G. Langdon, Microhardness evolution and mechanical characteristics of commercial purity titanium processed by high-pressure torsion, Mater. Sci. Eng. A 614 (2014) 223-231.

[30] P. Kumar, M. Kawasaki, T.G. Langdon, Review: Overcoming the paradox of strength and ductility in ultrafine-grained materials at low temperatures, J. Mater. Sci. 51 (2016) 7-18.

[31] R.B. Figueiredo, P.R. Cetlin, T.G. Langdon, Using finite element modeling to examine the flow processes in quasi-constrained high-pressure torsion, Mater. Sci. Eng. A 528 (2011) 8198-8204.

[32] R.B. Figueiredo, P.H.R. Pereira, M.T.P. Aguilar, P.R. Cetlin, T.G. Langdon, Using finite element modeling to examine the temperature distribution in quasi-constrained high-pressure torsion, Acta Mater. 60 (2012) 3190-3198.

[33] P.H.R. Pereira, Y. Huang, T.G. Langdon, Examining the mechanical properties and superplastic behaviour in an Al-Mg-Sc alloy after processing by HPT, Lett. Mater. 5 (2015) 294-300.

[34] S.K. Sikka, Y.K. Vohra, R. Chidambaram, Omega phase in Materials, Prog. Mater. Sci. 27 (1982) 245-310.

[35] B.D. Cullity, S.R. Stock, *Elements of X-ray Diffraction*, 3rd ed, Prentice Hall, Englewood Cliffs, NJ, U.S.A., 2001.

[36] J. Wang, Z. Horita, M. Furukawa, M. Nemoto, N.K. Tsenev, R.Z. Valiev, Y. Ma, T.G. Langdon, An investigation of ductility and microstructural evolution in an Al-3% Mg alloy with submicron grain size, J. Mater. Res. 8 (1993) 2810-2818.

[37] W. Huang, X. Zan, X. Nie, M. Gong, Y. Wang, Y. Xia, Experimental study on the dynamic tensile behavior of a poly-crystal pure titanium at elevated temperatures, Mater. Sci. Eng. A 443 (2007) 33-41.

[38] F.J. Humphreys, M. Hatherly, *Recrystallization and Related Annealing Phenomena*, Elsevier, Amsterdam, The Netherlands, 2004.

[39] T.G. Langdon, An evaluation of the strain contributed by grain boundary sliding in superplasticity, Mater. Sci. Eng. A 174 (1994) 225-230.

[40] A. Varloteaux, J. J. Blandin, M. Suéry, Control of cavitation during superplastic forming of high strength aluminium alloys, Mater. Sci. Tech. 5 (1989) 1109-1117.

[41] A.T. Santhanam, R.E. Reed-Hill, The influence of strain rate dependent work hardening on the necking strain in α-titanium at elevated temperatures, Metall. Trans. 2 (1971) 2619-2622.

[42] A.M. Garde, A.T. Santhanam, R.E. Reed-Hill, The significance of dynamic strain aging in titanium, Acta Metall. 20 (1972) 215-220.

[43] T. G. Langdon, Seventy-five years of superplasticity: Historic developments and new opportunities, J. Mater. Sci. 44 (2009) 5998-6010.

Figures captions

Fig. 1. (a) Values of the microhardness versus distance from the centres of the disks: the lower dashed line shows the annealed condition, and (b) X-ray patterns near the edges of the disks after HPT processing for various numbers of turns at a rotation rate of 1 rpm.

Fig. 2. (a) Optical micrograph of the microstructure after annealing at 973 K for 2 h followed by cooling in the furnace and (b) STEM image after 10 turns of HPT processing.

Fig. 3. Stress-strain curves at an initial strain rate of 1.0×10^{-3} s^{-1} in the annealed condition and after HPT for various numbers of turns.

Fig. 4. Stress-strain curves at different temperatures at an initial strain rate of 1.0×10^{-3} s^{-1} for (a) 10 turns of HPT processing and (b) the annealed condition.

Fig. 5. (a) Ultimate tensile strength and (b) elongation to failure of annealed and HPT-processed samples as a function of temperature after 10 turns.

Fig. 6. (a) Non-Isothermal (scanning) DSC measurements after HPT processing for 10 turns with a heating rate of 10 K min^{-1} and (b) Vickers microhardness in the grip area as a function of temperature after 10 turns of HPT: the lower dashed line denotes the hardness in the annealed condition.

Fig. 7. SEM images in the gauge areas after tensile testing at (a) 673, (b) 773 and (c) 873 K with an initial strain rate of 1.0×10^{-3} s^{-1} for samples processed by HPT through 10 turns: arrows in the microstructure at 773 K show the presence of small cavities.

Fig. 8. EBSD-orientation images in the grip (left) and gauge (right) areas after tensile testing at (a, b) 673, (c, d) 773 and (e, f) 873 K with an initial strain rate of 1.0×10^{-3} s^{-1}.

Fig. 9. Pictorial representation of the microstructural changes in nanocrystalline CP-Ti during

deformation at elevated temperatures (T>573 K): the diameter of each microstructural image is 10 μm. The sample tested at 773 K shows the minimum elongation to failure.

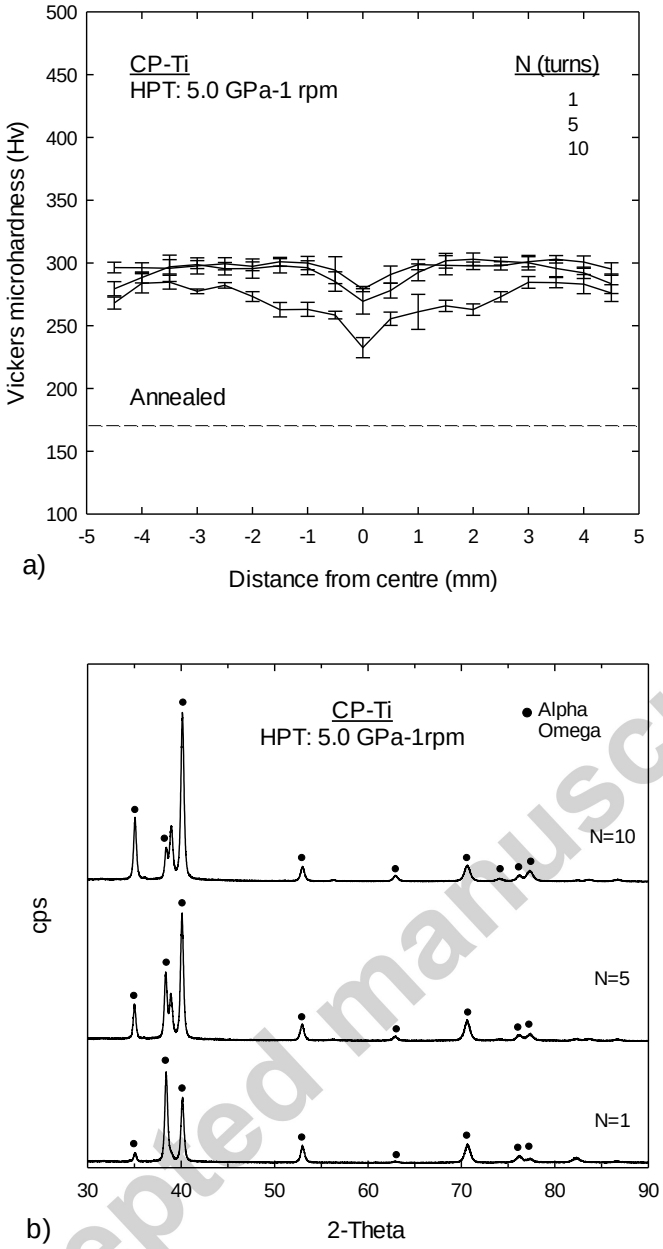

Fig. 1. (a) Values of the microhardness versus distance from the centres of the disks: the lower dashed line shows the annealed condition, and (b) X-ray patterns near the edges of the disks after HPT processing for various numbers of turns at a rotation rate of 1 rpm.

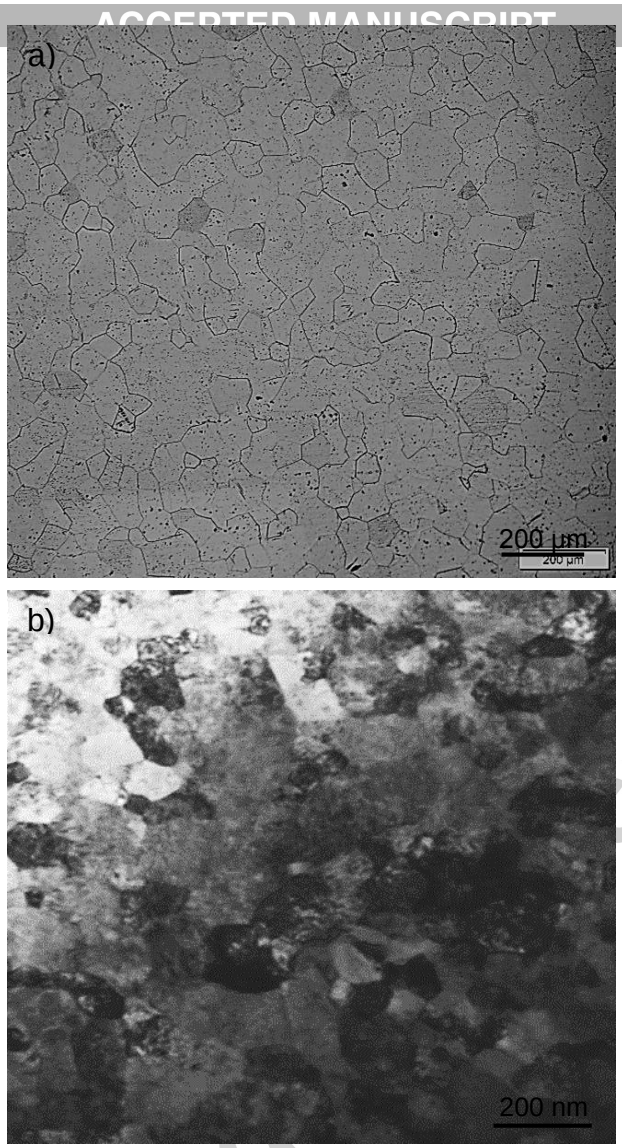

Fig. 2. (a) Optical micrograph of the microstructure after annealing at 973 K for 2 h followed by cooling in the furnace and (b) STEM image after 10 turns of HPT processing.

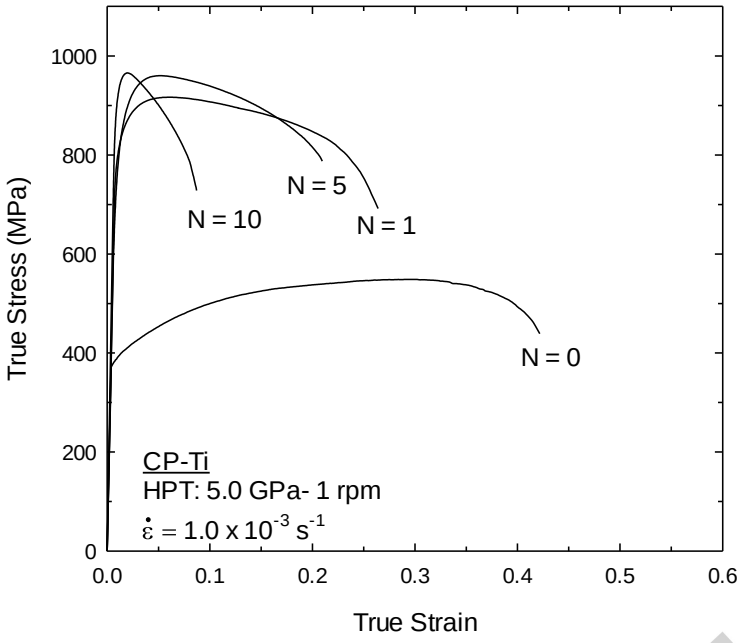

Fig. 3. Stress-strain curves at an initial strain rate of 1.0 ×10^{-3} s^{-1} in the annealed condition and after HPT for various numbers of turns.

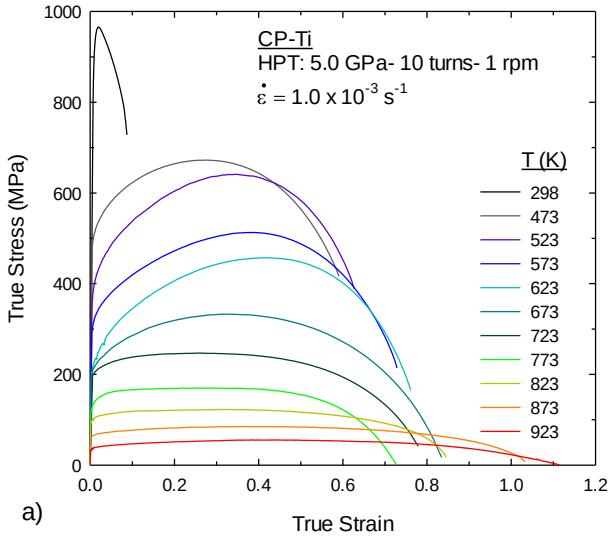

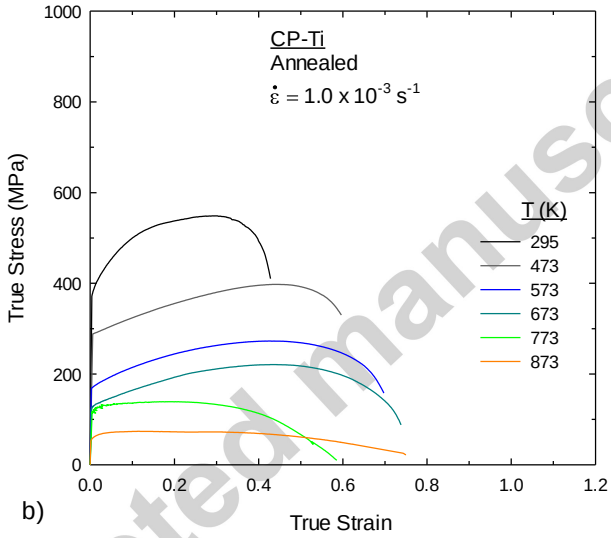

Fig. 4. Stress-strain curves at different temperatures at an initial strain rate of 1.0×10^{-3} s^{-1} for (a) 10 turns of HPT processing and (b) the annealed condition.

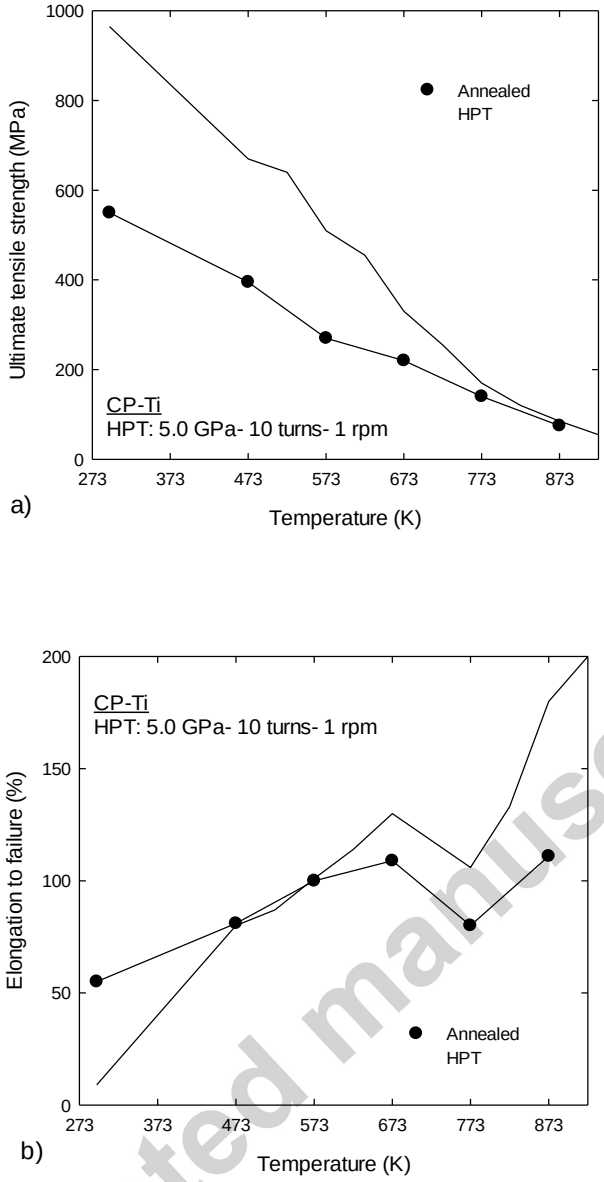

Fig. 5. (a) Ultimate tensile strength and (b) elongation to failure of annealed and HPT-processed samples as a function of temperature after 10 turns.

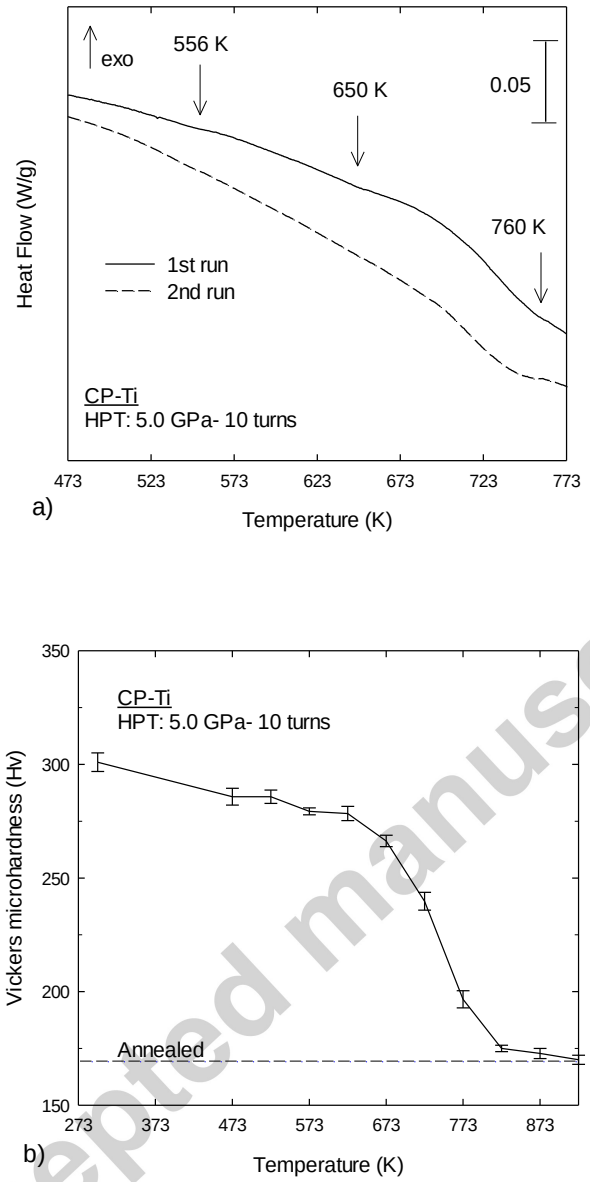

Fig. 6. (a) Non-Isothermal (scanning) DSC measurements after HPT processing for 10 turns with a heating rate of 10 K min^{-1} and (b) Vickers microhardness in the grip area as a function of temperature after 10 turns of HPT: the lower dashed line denotes the hardness in the annealed condition.

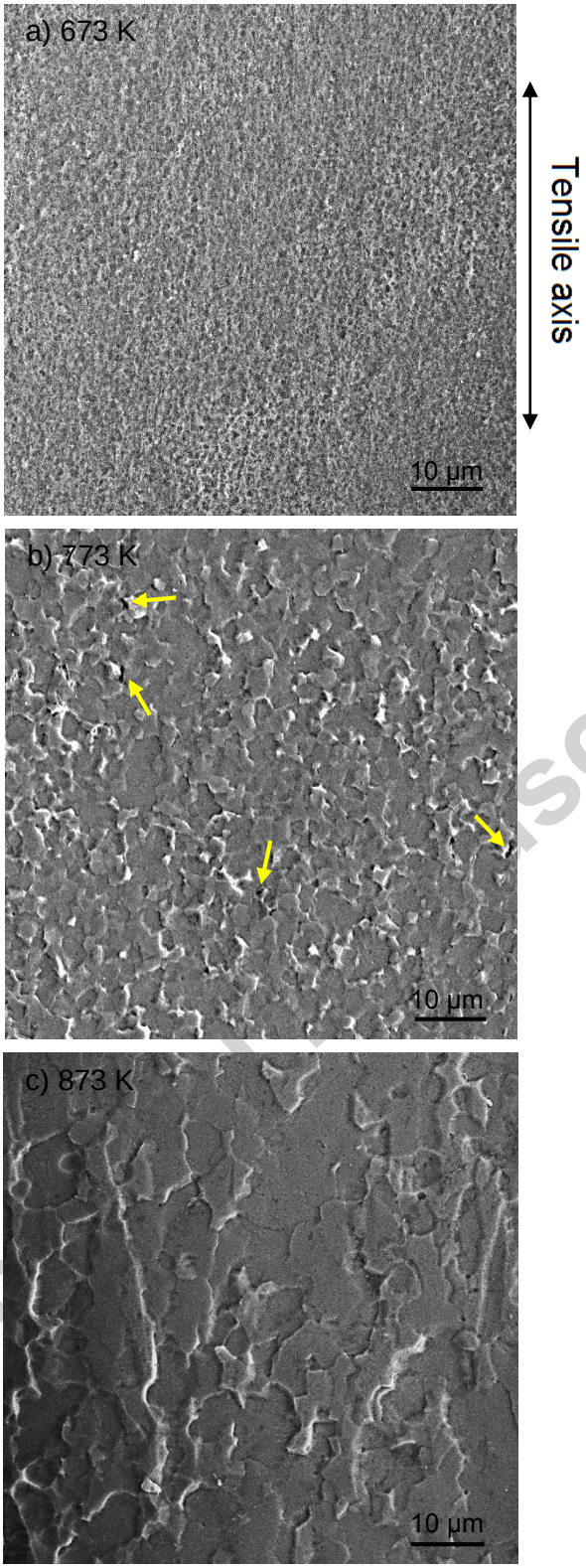

Fig. 7. SEM images in the gauge areas after tensile testing at (a) 673, (b) 773 and (c) 873 K with an initial strain rate of 1.0×10^{-3} s^{-1} for samples processed by HPT through 10 turns: arrows in the microstructure at 773 K show the presence of small cavities.

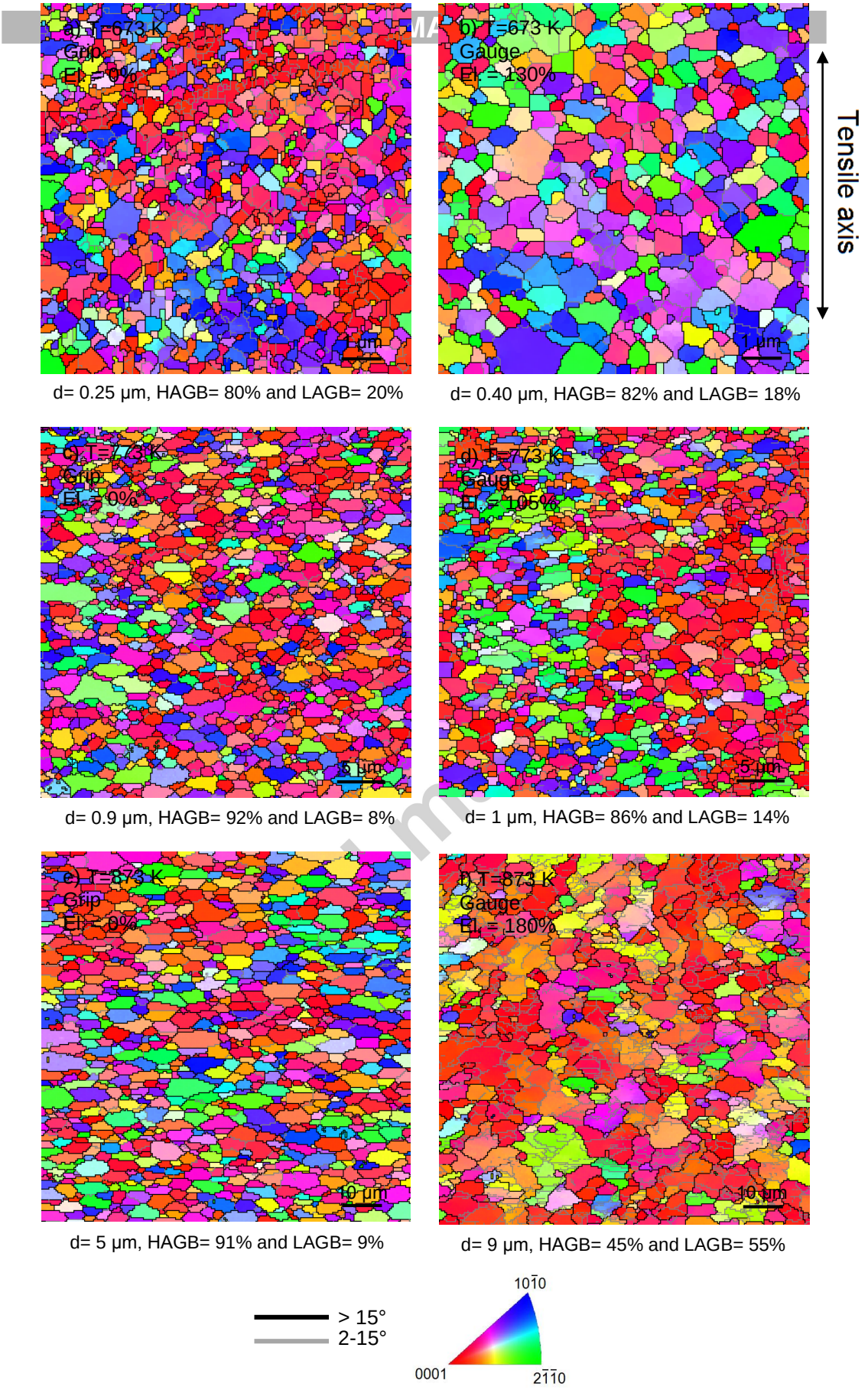

Fig. 8. EBSD-orientation images in the grip (left) and gauge (right) areas after tensile testing at (a, b) 673, (c, d) 773 and (e, f) 873 K with an initial strain rate of 1.0×10^{-3} s^{-1}.

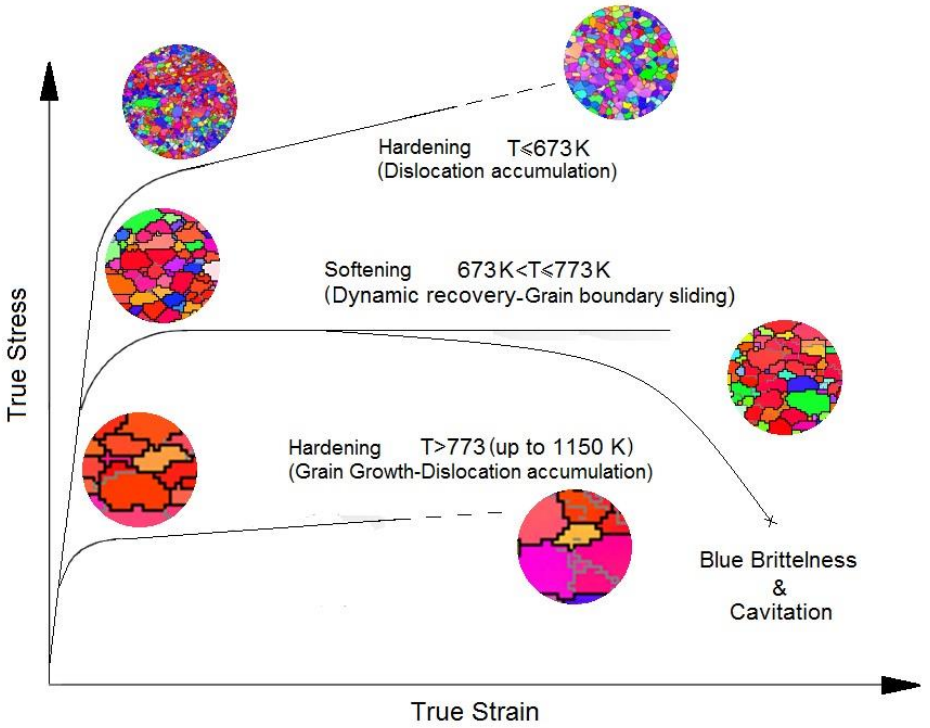

Fig. 9. Pictorial representation of the microstructural changes in nanocrystalline CP-Ti during deformation at elevated temperatures (T>573 K): the diameter of each microstructural image is 10 μm. The sample tested at 773 K shows the minimum elongation to failure.